Supplemental Information for

Highly efficient sky-blue light-emitting diodes based on Cu-treated halide perovskite nanocrystals

Fang Chen [a,b], Leimeng Xu [c], Yan Li [c], Tao Fang [c], Tiantian Wang [c], Marco Salerno[a], Mirko Prato*[a] and Jizhong Song*[c,d]

a. Materials Characterization Facility, Istituto Italiano di Tecnologia, Via Morego 30, Genova 16163, Italy.

b. Dipartimento di Chimica e Chimica Industriale, Università degli Studi di Genova, Via Dodecaneso 31, 16146 Genova, Italy.

c. MIIT Key Laboratory of Advanced Display Materials and Devices, School of Materials Science and Engineering, Nanjing University of Science and Technology, Nanjing 210094, China.

d. School of Physics and Microelectronics, Zhengzhou University, Zhengzhou 450052, China.

* Emails of corresponding authors: mirko.prato@iit.it, songjizhong@njust.edu.cn.

Table S1. Statistics of performance metrics of HP sky-blue LEDs from literatures and the current work. (TF: thin film)

| Type	Material	Turn-on voltage (V)@cd/m2	Max Lum (cd/m2)	Max EQE (%)	CE (cd/A)	Max PE (lm/W)	Lum@Max EQE (cd/m2)	J@MaxEQE (mA/cm2)	EL peak (nm)	FWHM (nm)	Ref.
3D TF	$MAPbBr_{1.08}Cl_{1.92}$	~3.3	~1.75	~0.0003	~0.00035	/	~1.65	~650	482	~20	[1]
	$Rb_xCs_{1-x}PbBr_{3-y}Cl_y$	~3.3	244	0.17	0.32	/	~7	~2	492	~20	[2]
	$PEA_{0.2}Cs_{0.4}MA_{0.6}Pb_{0.85}Mn_{0.15}(BrCl)_3$	~4.5	11800	0.58	/	/	~70	~90	~495	/	[3]
2D TF	$(EA)_2(MA)_{n-1}Pb_nBr_{3n+1}$	2.7	70	2.6	/	~3.8	~0.02	0.5	473, 485	~50	[4]
	$IPA/PEA_2MA/Cs_{n-1}PbnBr_{3n-1}$(80nm)	~7.1	~400	1.5	2.8	0.92	~280	8	490	28	[5]
	$IPA/PEA_2MA/Cs_{n-1}PbnBr_{3n-1}$(40nm)	~5.4	2480	~1	~1.9	~0.8	~500	30	490	28	[5]
	$BA_2Cs_{n-1}Pb_n(BrCl)_{3n+1}$	4.5	~3000	6.2	~7	~2.5	3340	~45	487	/	[6]
Quasi-2D TF	$(4-PBA)_2PbBr_4:CsPbBr_3$	2.9	186	0.015	/	/	186	600	491	/	[7]
	$KBr:PA_2(CsPbBr_3)_{n-1}PbBr_4$	3.31	4359	1.45	2.25	/	4359	40	492	26	[8]
	$KBr:PA_2(CsPbBr_3)_{n-1}PbBr_4$	/	5737	1.07	/	/	5737	/	492	26	[8]
	$100\%PEABr/CsPbCl_{0.9}Br_{2.1}$	3.2	3780	5.7	6.1	/	700	10	480	21	[9]
	$RbBr:PEA_2(Rb_{0.4}Cs_{0.6})_2Pb_3Br_{10}$	~3.5	854	1.48	/	/	~200	~4	490	~30	[10]
	$PBABr_{1.1}(Cs_{0.7}FA_{0.3}PbBr_3)$	3.3	800	9.5	12	/	54	~0.3	483	26	[11]
	$2\%YCl_3:PEACl:CsPbBr_3$	~3.3	9040	11	/	/	~600	~5	485	/	[12]
NP	$MAPbBr_3$	~3.5	<10	0.23	/	/	8.5	4.7	492	24	[13]
	$Cs[PbBr_6]^{4+}$	~4	48	0.55	1.1	0.19	/	<1	487	21	[14]
NC	$MAPbBr_xCl_{3-x}$	>7.8	2252	1.01	/	/	/	/	495	<30	[15]
	$CsPbBr_xCl_{3-x}$	~4.2	830	1.41	/	/	10.5	/	488	<25	[16]
	$Rb_xCs_{1-x}PbBr_3$	~4.2	186	0.87	/	/	93	~7	490	22	[17]
	$CsPbBr_{2.71}Cl_{0.19}$	~3	2063	3.5	/	/	~7	~0.06	490	~20	[18]
	Cu30-octane	~2.8	672	3.85	6.1	6	20	0.3	493	~19	Our work
	Cu30DDABDDAC	~2.6	1946	5.02	7.3	7.2	130	1.8	491	~20	Our work
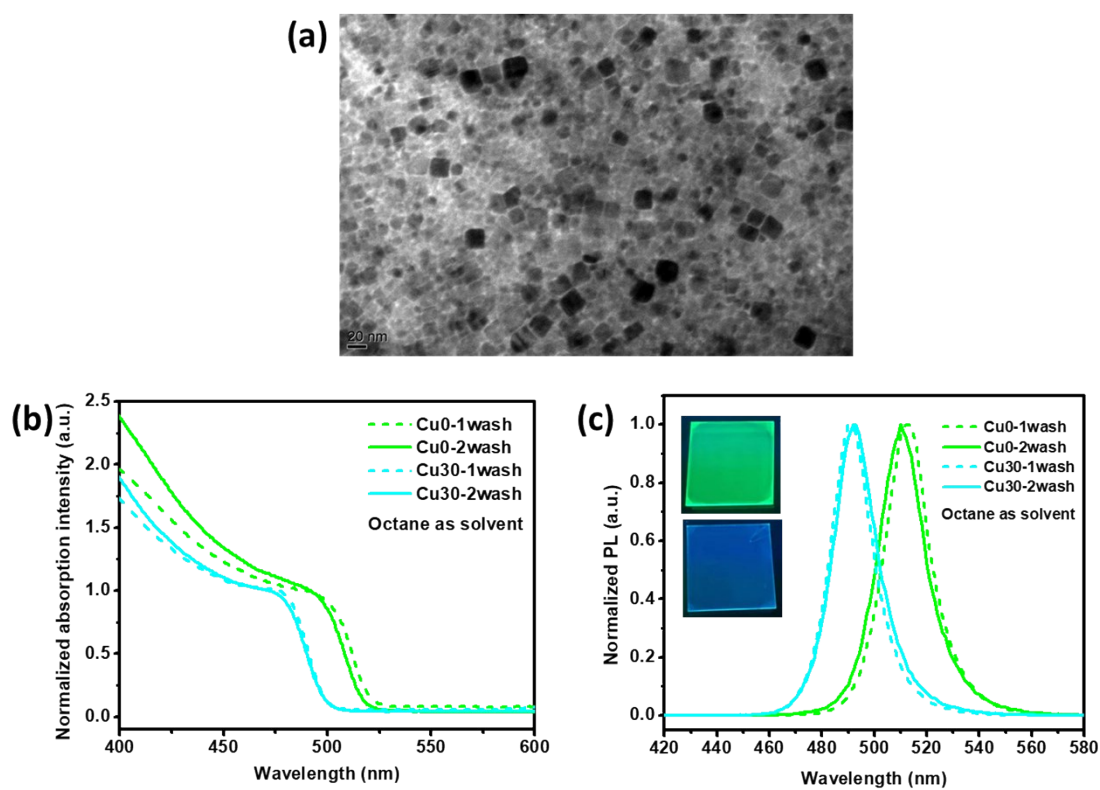
Figure S1. Characterization of Cu0 NCs and comparison with Cu30 NCs after washing with octane for different times. (a) TEM image of NCs without treatment of CuCl$_2$; Normalized (b) absorption spectra; and (c) PL spectra of the Cu0 and Cu30 NCs dissolved in octane after washing once or twice. Shown in the inset of (c) is the photos of the Cu0-2wash NC film (green) and the Cu30-2wash NC film (blue) under UV light.
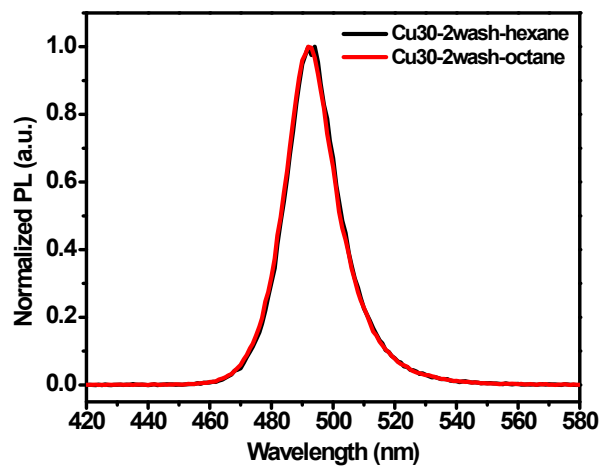
Figure S2. Normalized PL spectra of the Cu30-octane and Cu30-hexane NC solutions.
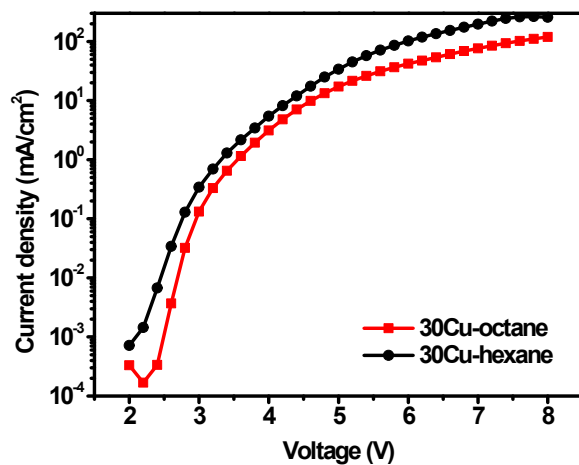
Figure S3. Comparison of current densities of the Cu30-octane LED and the Cu30-hexane LED as a function of applied voltage.
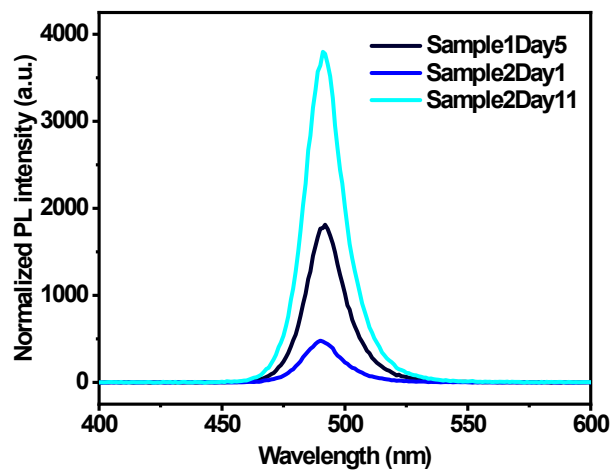
Figure S4. Comparison of normalized PL intensity of two Cu30 NC solutions aged for different days.
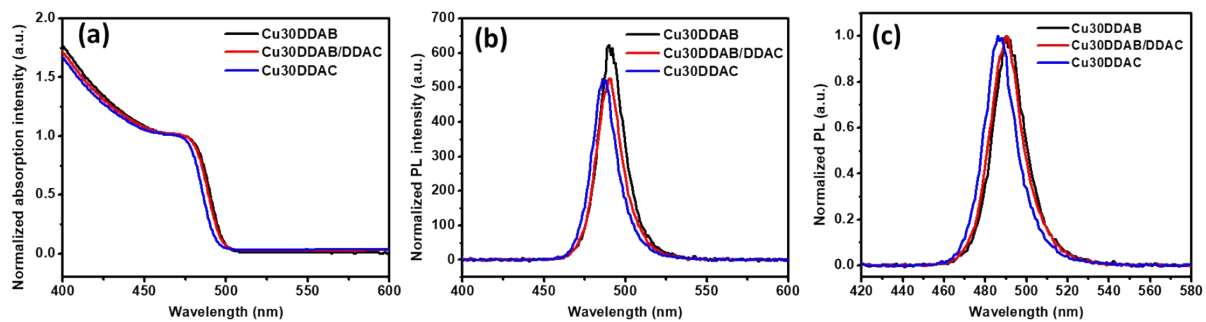
Figure S5. Effect of ligands on optical performance of Cu30 NCs. (a) Absorption spectra; (b) normalized PL intensity and (c) normalized PL spectra of the Cu30DDAB, Cu30DDABDDAC and Cu30DDAC NC solutions.
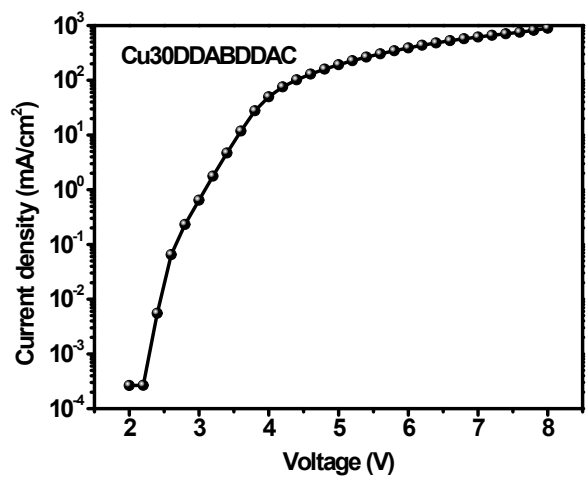
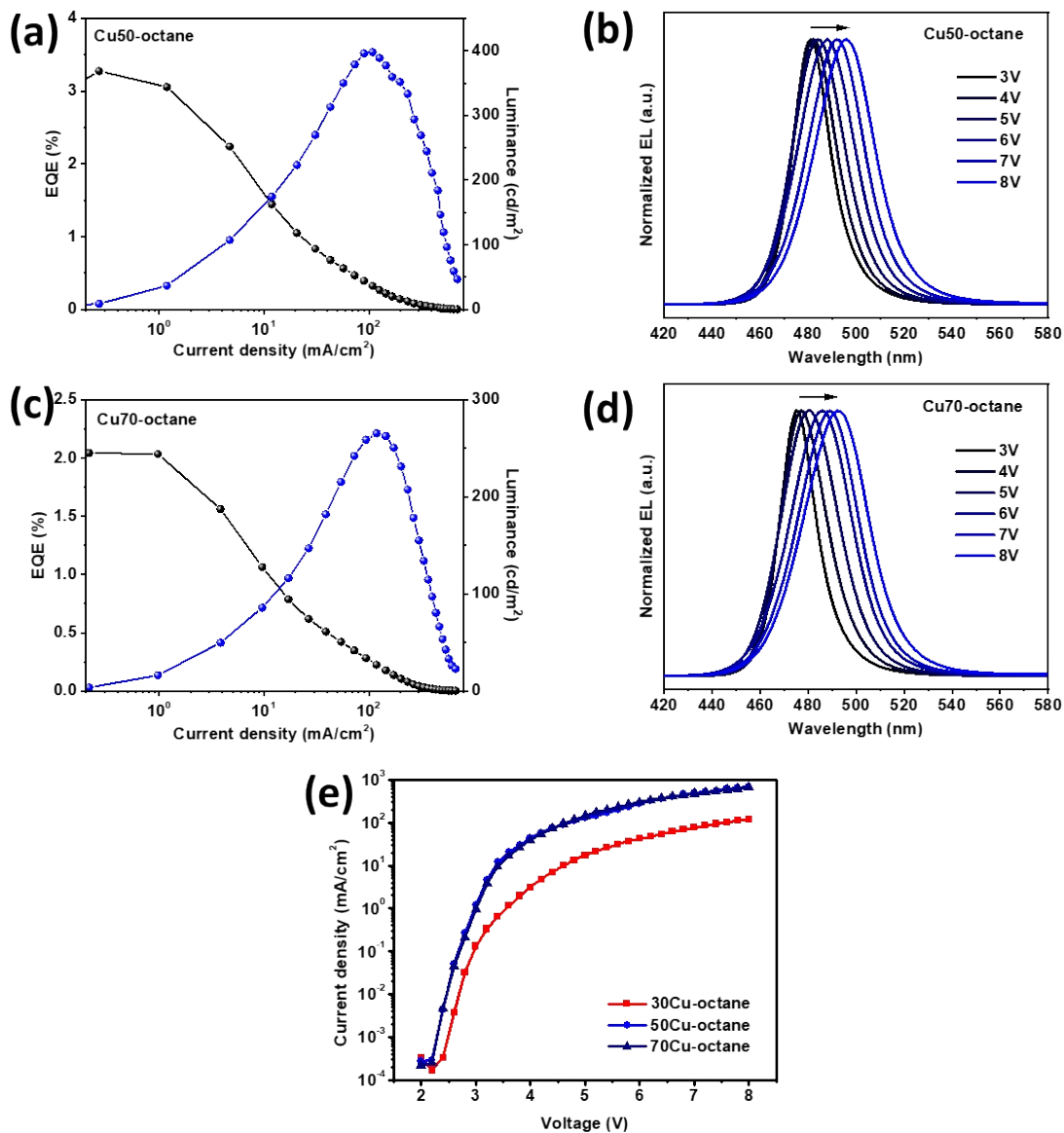**Figure S6.** Current density as a function of applied voltage.

Figure S7. Performance of Cu50-octane and Cu70-octane LEDs. (a) EQE and luminance as a function of current density; and (b) normalized EL spectra under increasing bias of the Cu50-octane LED. (c) EQE and luminance as a function of current density; and (d) normalized EL spectra under increasing bias of the Cu70-octane LED. (e) Comparison of current densities of the Cu30-octane LED, Cu50-octane LED and Cu70-octane LED as a function of applied voltage.

Table S2. Performance metrics of the HP NCs-based LEDs in the current work.

| Material	Turn-on voltage (V)	Max Lum (cd/m²)	Max EQE (%)	CE (cd/A)	Max PE (lm/W)	Lum@Max EQE (cd/m²)	J@MaxE QE (mA/cm²)	EL peak (nm)	FWHM (nm)	Average MaxEQEs (%)	Average MaxLum (cd/m²)
30-hexane	2.8	714	1.51	2.45	2.75	3	0.13	493	19	1.5	389.1
30Cu-octane	2.8	672	3.85	6.07	5.96	20	0.33	493	19	3.7	756.5
30Cu-Day10	2.8	692	4.02	6.54	6.85	8	0.12	494	18	3.7	670.3
30CuDDABD DAC	2.6	1946	5.02	7.31	7.17	130	1.78	490	19	4.9	1904.7
50Cu-octane	2.6	398	3.27	3.4	3.82	9	0.27	481	18	3.1	418.8
70Cu-octane	2.8	266	2.03	1.71	1.92	4	0.21	475	18	2	269.9
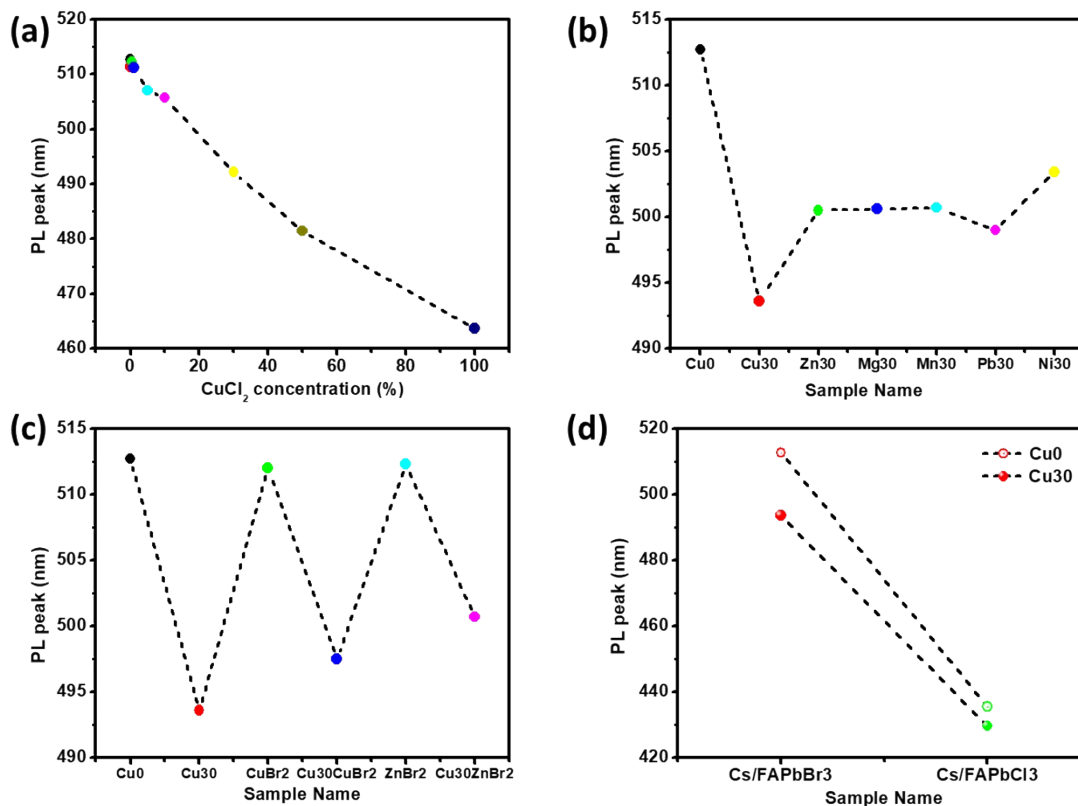
Figure S8. Study on the role of copper ions in Cu30 NCs. PL peaks of HP NCs treated with (a) different concentrations of CuCl$_2$; (b) different types of metal chlorides and (c) CuBr$_2$ or ZnBr$_2$; and (d) PL peaks of HP NCs with varying compositions of halide and treated with or without CuCl$_2$.

    To illustrate the possible mechanism of the blue shift of PL after the addition of CuCl$_2$, we carried out some series of control experiments. Firstly, we considered a series of different amount of CuCl$_2$ added into the reaction system and characterized the optical performance of the obtained NCs, labeled sequentially as Cu0, Cu0.1, Cu0.5, Cu1, Cu5, Cu10, Cu50 and Cu100, where the number indicates the molar percentage of Cu added to the Pb used in the synthesis. The PL peak keeps almost the same spectral position and FWHM, when the amount of CuCl$_2$ is no more than 1% of the mole amount of PbBr$_2$ (Figure S8). In contrast, when the amount of CuCl$_2$ is more than 5% of that of PbBr$_2$ used in the reaction system, the PL peak displays gradually enlarged blue shift, moving from 513 nm for the Cu0 NCs, up to 507 nm, 506 nm, 481 nm, and 464 nm for the Cu5, Cu10, Cu50, and Cu100 NCs, respectively. Actually, our results (Figure 4a) are consistent with the effect of anion exchange as reported in the literature, where it

was reported to have a non-linear relation to the concentration [1]. Thus, we foresee three possible explanations for the blue shift of the PL peak of the NCs after treatment with $CuCl_2$. The first one, and most plausible, is that there may be anion exchange between bromide and chloride, which has been reported to be thermodynamically favorable.[2] The second one is that the presence of copper ions cations may be able to favor the anion exchange,[3] when $CuCl_2$ concentration in the reaction system is beyond a certain threshold. The third one is that the copper ions may be doped inside the NCs, which is reported to be able to cause lattice contraction and further enlarged bandgap.[4]

To understand the role of Cu, we treated our NC solutions with different metal chlorides at a fixed molar ratio of 30% vs. $PbBr_2$. The samples are individually labeled as Zn30, Mg30, Mn30, Pb30, and Ni30, where each label indicates the metal of the used chloride. All treated NC solutions show blue-shifted PL peaks (Figure 4b and Figure S9a), among which Zn30, Mg30, Mn30, and Pb30 NCs present a blue shift of ~12 nm relative to the Cu0 NCs. Ni30 presents ~10 nm blue shift. In contrast, the PL peak of the Cu30 NCs displays a blue shift of ~20 nm as compared to the PL peak of the Cu0 NCs, with PL FWHM ~1 nm smaller than those of the other treated NCs. The higher blue shift of the PL peak of the Cu30 NCs may be explained by the assuming indeed that copper ions might have favored the anion exchange reaction between Cl^- of the added salt and the Br^- in the NCs. Experimental results on co-doping of $ZnCl_2$, $MgCl_2$, or $MnCl_2$ with $CuCl_2$ also confirm this. For instance, the PL peak of the Cu50 NCs is even bluer than the PL peak of the Cu30Zn30, Cu30Mg30, and Cu30Mn30 NCs (Figure S9b,c), although there is less chloride in the reaction system for the Cu50 NCs.

In order to figure out whether the effect of PL shift could be ascribed also to copper ions doped into the NCs, on one hand, we treated the as-synthesized NCs with either $CuBr_2$ or $ZnBr_2$, or with a mixture of the same salts and $CuCl_2$. However, the PL peak position of the NCs obtained after treatment with $CuBr_2$ or $ZnBr_2$[5] alone is the same as that of the untreated sample (Figure 4c and Figure S10). This is most likely due to the absence of anion exchange between the NCs and the added salts, which is reported to be necessary for metal doping inside HP NCs.[6, 7] In contrast, the NCs treated with $CuBr_2$ or $ZnBr_2$ in addition to $CuCl_2$, display blue-shifted PL peak. The PL peak of the Cu30-$CuBr_2$ NCs is more blue-shifted than that of the Cu30-$ZnBr_2$ NCs. Considering that the same amount of bromide should be present in both reaction systems,

this observation strongly suggests that not only anion exchange but also copper ions is playing a significant role, maybe by doping the NCs.

On the other hand, $CuCl_2$ was used to treat not only $Cs_xFA_{1-x}PbBr_3$ NCs, but also similarly-synthesized $Cs_xFA_{1-x}PbCl_3$ NCs during post-synthesis, with the Cu/Pb molar ratios set at 0.3:1. The addition of $CuCl_2$ leads to a blue shift of the PL peak in all the systems (Figure 4d and Figure S11). In particular, we observed a blue-shift of ~6 nm in the PL of $Cs_xFA_{1-x}PbCl_3$ NCs after treatment with $CuCl_2$ and DDAB. The Br⁻ in DDAB could have induced anion exchange, but this would have caused a redshift of the PL peak. On the other hand, the anion exchange could have acted as a boost for the copper doping in this system.[6] Chen *et al.* observed a 2-nm PL blue shift of $CsPbCl_3$ NCs during treatment with $CuCl_2$, and attributed it to the change of the dielectric constant due to existence of copper ions in solution and on NC surface.[3] Here, considering that the blue shift in our case is much larger, even in the presence of Br⁻ from DDAB, we attribute it to doping of copper ions into the NCs rather than merely absorbing on NC surface. Thus, the blue shift of the PL peak of the Cu30 NCs in comparison with the Cu0 NCs could be attributed to a combination of anion exchange enhanced by copper ions and doping of copper ions into NCs.
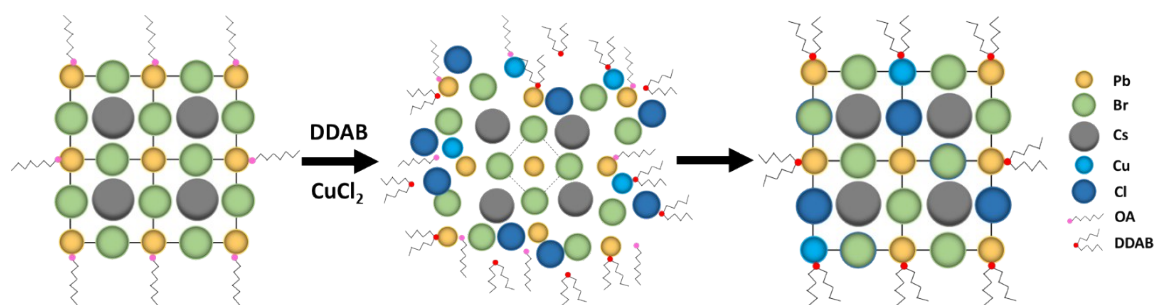
Figure S9. A scheme of the reaction mechanism of NC post-synthesis after the addition of CuCl$_2$ and DDAB into crude NC solutions.

Based on the observations, we speculate that after the addition of CuCl$_2$:DDAB:toluene solution, the initial NCs disintegrate and re-dissolve into the solvent. With increasing reaction time, lead bromide and/or chloride octahedra re-connect to each other and re-crystallize, together with inclusion of some copper ions into the NCs and oleic acid (OA) ligands replaced by copper and DDAB, respectively, obtaining the final Cu30 NCs. In this way, rather than adding CuCl$_2$ during other stages, the prepared Cu30 NCs could stay stable, without precipitates, for more than half a year.
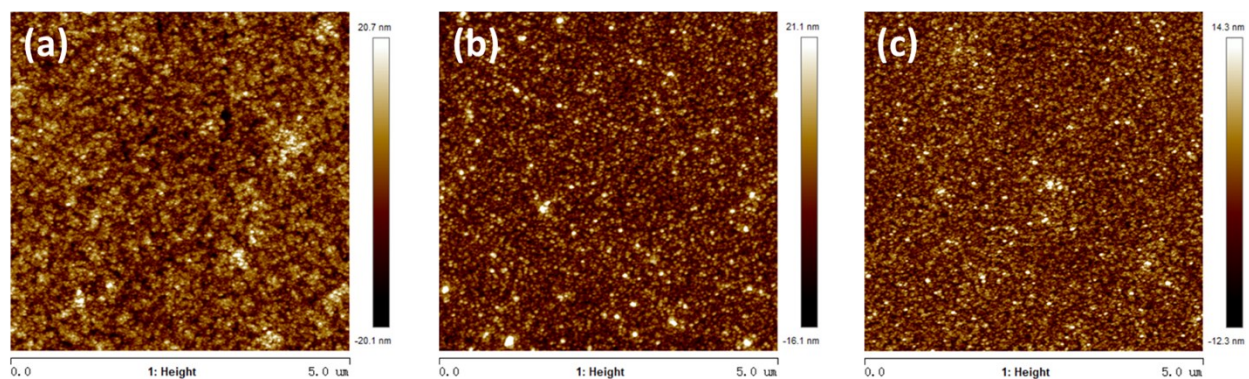
Figure S10. Surface topography of the NC films. AFM image of (a) Cu30-hexane; (b) Cu30-octane; and (c) Cu30DDABDDAC films.

Table S3. Roughness of the NC films corresponding to the AFM images.

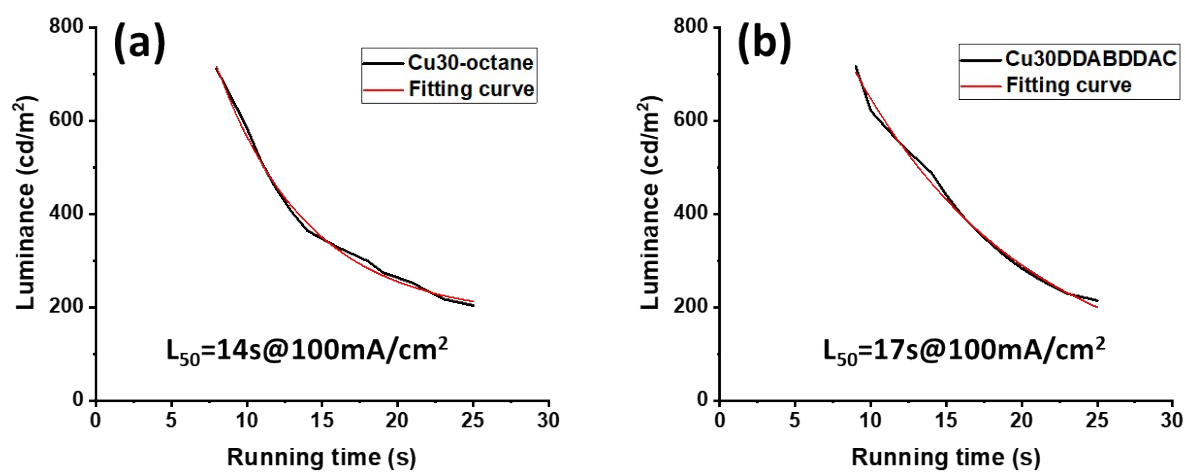| Film	Cu30-octane	Cu30-hexane	Cu30DDABDDAC
Roughness (nm)	4.50	3.99	2.93

Figure S11. Half-lifetime (L50) of the running devices. Exponential fitting curves of L50 of (a) Cu30-octane LED and (b) Cu30DDABDDAC LED, which are operated at a constant current density of 100 mA/cm^2.
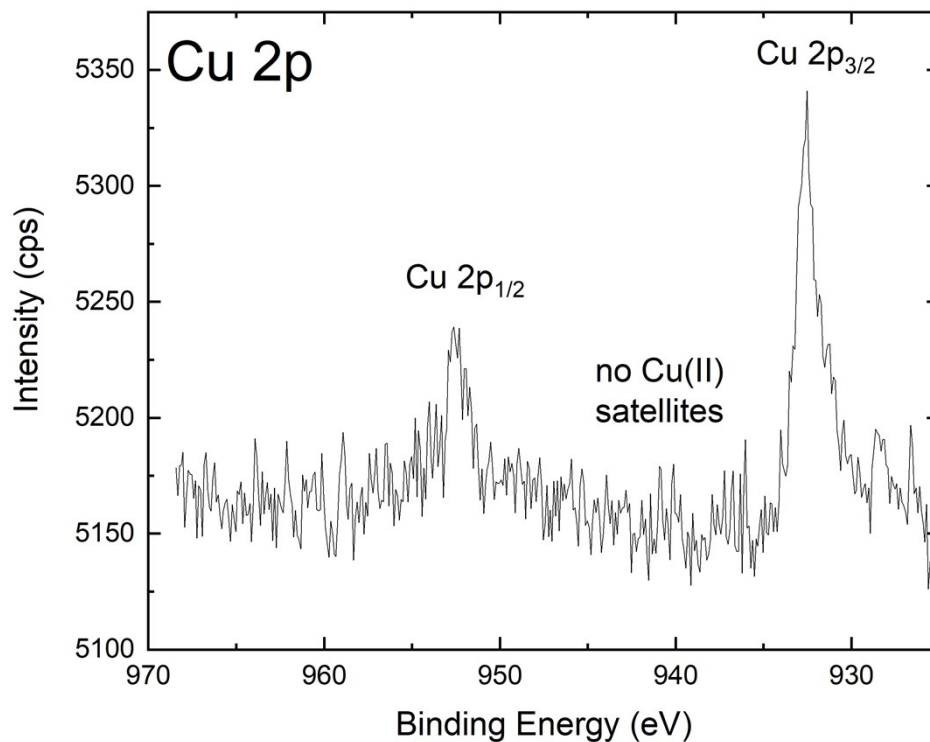
Figure S12. Cu 2p XPS peaks measured on the Cu30 sample. The main peak is centered at (932.6±0.3) eV. Together with the absence of the typical Cu(II) satellites in the 940 - 950 eV range,[26] the data support the presence of Cu(I) in the system.

References

1. N. K. Kumawat, A. Dey, A. Kumar, S. P. Gopinathan, K. L. Narasimhan and D. Kabra, *ACS Applied Materials & Interfaces*, 2015, **7**, 13119-13124.
2. H. Wang, X. Zhao, B. Zhang and Z. Xie, *Journal of Materials Chemistry C*, 2019, **7**, 5596-5603.
3. M. K. Gangishetty, S. N. Sanders and D. N. Congreve, *ACS Photonics*, 2019, **6**, 1111-1117.
4. Q. Wang, J. Ren, X.-F. Peng, X.-X. Ji and X.-H. Yang, *ACS Applied Materials & Interfaces*, 2017, **9**, 29901-29906.
5. J. Xing, Y. Zhao, M. Askerka, L. N. Quan, X. Gong, W. Zhao, J. Zhao, H. Tan, G. Long, L. Gao, Z. Yang, O. Voznyy, J. Tang, Z.-H. Lu, Q. Xiong and E. H. Sargent, *Nature Communications*, 2018, **9**, 3541.
6. P. Vashishtha, M. Ng, S. B. Shivarudraiah and J. E. Halpert, *Chemistry of Materials*, 2019, **31**, 83-89.
7. L. Cheng, Y. Cao, R. Ge, Y.-Q. Wei, N.-N. Wang, J.-P. Wang and W. Huang, *Chinese Chemical Letters*, 2017, **28**, 29-31.
8. Z. Ren, X. Xiao, R. Ma, H. Lin, K. Wang, X. W. Sun and W. C. H. Choy, *Advanced Functional Materials*, 2019, **29**, 1905339.
9. Z. Li, Z. Chen, Y. Yang, Q. Xue, H.-L. Yip and Y. Cao, *Nature Communications*, 2019, **10**, 1027.
10. Y. Jiang, C. Qin, M. Cui, T. He, K. Liu, Y. Huang, M. Luo, L. Zhang, H. Xu, S. Li, J. Wei, Z. Liu, H. Wang, G.-H. Kim, M. Yuan and J. Chen, *Nature Communications*, 2019, **10**, 1868.
11. Y. Liu, J. Cui, K. Du, H. Tian, Z. He, Q. Zhou, Z. Yang, Y. Deng, D. Chen, X. Zuo, Y. Ren, L. Wang, H. Zhu, B. Zhao, D. Di, J. Wang, R. H. Friend and Y. Jin, *Nature Photonics*, 2019, **13**, 760-764.
12. Q. Wang, X. Wang, Z. Yang, N. Zhou, Y. Deng, J. Zhao, X. Xiao, P. Rudd, A. Moran, Y. Yan and J. Huang, *Nature Communications*, 2019, **10**, 5633.
13. S. Kumar, J. Jagielski, S. Yakunin, P. Rice, Y.-C. Chiu, M. Wang, G. Nedelcu, Y. Kim, S. Lin, E. J. G. Santos, M. V. Kovalenko and C.-J. Shih, *ACS Nano*, 2016, **10**, 9720-9729.
14. R. L. Z. Hoye, M.-L. Lai, M. Anaya, Y. Tong, K. Gałkowski, T. Doherty, W. Li, T. N. Huq, S. Mackowski, L. Polavarapu, J. Feldmann, J. L. MacManus-Driscoll, R. H. Friend, A. S. Urban and S. D. Stranks, *ACS Energy Letters*, 2019, **4**, 1181-1188.
15. W. Deng, X. Xu, X. Zhang, Y. Zhang, X. Jin, L. Wang, S.-T. Lee and J. Jie, *Advanced Functional Materials*, 2016, **26**, 4797-4802.
16. M. K. Gangishetty, S. Hou, Q. Quan and D. N. Congreve, *Advanced Materials*, 2018, **30**, 1706226.
17. P. Todorović, D. Ma, B. Chen, R. Quintero-Bermudez, M. I. Saidaminov, Y. Dong, Z.-H. Lu and E. H. Sargent, *Advanced Optical Materials*, 2019, **7**, 1901440.
18. Y. Shynkarenko, M. I. Bodnarchuk, C. Bernasconi, Y. Berezovska, V. Verteletskyi, S. T. Ochsenbein and M. V. Kovalenko, *ACS Energy Letters*, 2019, **4**, 2703-2711.
19. Q. A. Akkerman, V. D'Innocenzo, S. Accornero, A. Scarpellini, A. Petrozza, M. Prato and L. Manna, *Journal of the American Chemical Society*, 2015, **137**, 10276-10281.
20. W. Lv, X. Tang, L. Li, L. Xu, M. Li, R. Chen and W. Huang, *The Journal of Physical Chemistry C*, 2019, **123**, 24313-24320.
21. Y.-C. Chen, H.-L. Chou, J.-C. Lin, Y.-C. Lee, C.-W. Pao, J.-L. Chen, C.-C. Chang, R.-Y. Chi, T.-R. Kuo, C.-W. Lu and D.-Y. Wang, *The Journal of Physical Chemistry C*, 2019, **123**, 2353-2360.
22. C. Bi, S. Wang, Q. Li, S. V. Kershaw, J. Tian and A. L. Rogach, *The Journal of Physical Chemistry Letters*, 2019, **10**, 943-952.
23. J. Song, T. Fang, J. Li, L. Xu, F. Zhang, B. Han, Q. Shan and H. Zeng, *Adv Mater*, 2018, **30**, e1805409.
24. A. Shapiro, M. W. Heindl, F. Horani, M.-H. Dahan, J. Tang, Y. Amouyal and E. Lifshitz, *The Journal of Physical Chemistry C*, 2019, **123**, 24979-24987.
25. S. Das Adhikari, S. K. Dutta, A. Dutta, A. K. Guria and N. Pradhan, *Angewandte Chemie International Edition*, 2017, **56**, 8746-8750.

26. M.C. Biesinger, *Surface and Interface Analysis*, **49** (2017) 1325-1334.